Electronic Supplementary Material (ESI) for Physical Chemistry Chemical Physics.

Supporting Information

Title: Low-index dielectric metasurfaces supported by metallic substrates for efficient second-harmonic generation in the blue-ultraviolet

*Kwang-Hyon Kim**

*Corresponding Author: E-mail: kwang-h.kim@star-co.net.kp

S1. Optical responses and second-harmonic generation from a metasurface of lithium niobate nanodisks supported by silica substrate

In order to identify the role of metallic substrate, here we study the optical responses of a metasurface consisting lithium niobate (LN) nanodisk array supported by dielectric substrate. Figure S1a illustrates the intensity enhancement in LN nanodisks when using silica substrate for structural parameters the same as in Figure 2 ($D = 260$ nm and $h = 120$ nm). The figure shows that the local field is much weaker than the case of using metallic substrate and optical resonances do not appear, which can also be confirmed from the reflection R and transmission spectra T shown in Figure S1b.

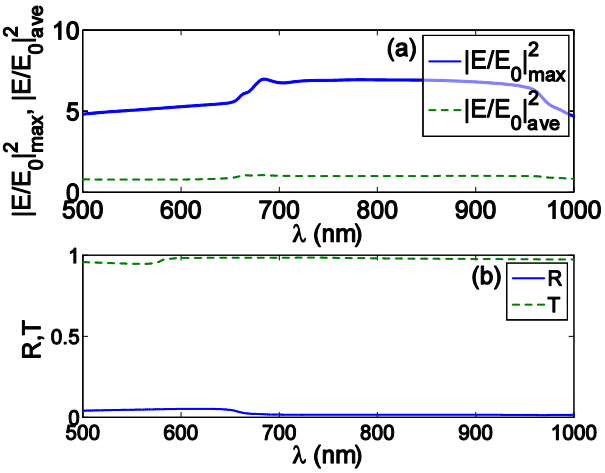

Figure S1. Optical responses of a metasurface of lithium niobate (LN) nanodisks supported by silica substrate. In (a), maxium $|E/E_0|^2_{max}$ and average intensity enhancements $|E/E_0|^2_{ave}$ in LN nanodisks are presented. In (b), reflection R and transmission spectra T are shown. The diameter and height of the nanodisks are $D = 260$ nm and $h = 120$ nm as in Figure 2.

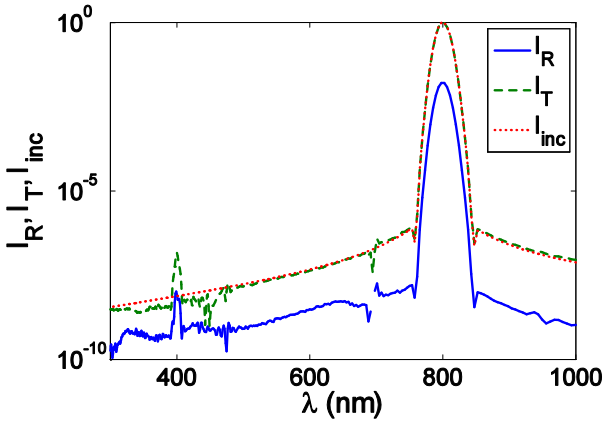

Figure S2. Pump I_{inc}, reflection I_R, and transmission I_T spectra for the metasurface shown in Figure S1. Pumping conditions are the same as in Figure 5.

Due to the low field enhancement, the above metasurface generates second-harmonic wave at 400 nm with significantly low efficiency: second-harmonic generation (SHG) efficiency for the reflected component amounts to $\eta_R = 1.44 \times 10^{-6}$ % and for transmitted component $\eta_T = 1.91 \times 10^{-5}$ % under pumping condition the same as in Figure 5, which are 2-3 orders-of-magnitude lower than the case of using gold substrate (see Figure 5).

S2. Multipole analysis for LN nanodisk array supported by gold substrate

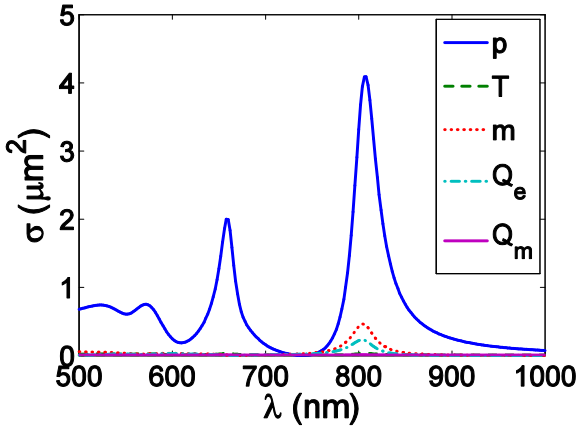

Figure S3. Contributions of electromagnetic multipoles of different orders to the scattering cross-section of individual nanodisks of the metasurface shown in Fig. 2. In the inset, p, T, m, Q_e, and

Q_m represent the contributions of electric dipole, toroidal dipole, magnetic dipole, electric quadrupole, and magnetic quadrupole, respectively.

Here we present the result of multipole analysis for LN nanodisk on gold substrate shown in Fig. 2. For this purpose, we calculate the contributions of multipoles to the scattering cross-section of the nanodisk in a unit cell of the metasurface, which are evaluated by using the formulas presented in [S1,S2]. Multipole decomposition result shows that the electric dipole provides the major contribution to the resonant electromagnetic response of the metasurface.

S3. Optical responses and second-harmonic generation from a single lithium niobate nanodisk placed on gold substrate

Intensity enhancement of an isolated LN nanodisk placed on gold substrate has a peak at 782 nm (Figure S4a), originating from the dipolar plasmonic resonance which can be confirmed from Figure S4b. Compared with the case of LN metasurface, the averaged intensity in the nanodisk is much weaker and most of the energy is confined in the vicinity of the interface between the LN nanodisk and gold substrate (Figure S4b), which clearly reveals that the high field enhancement in the case of LN metasurface is the result of collective resonance in LN nanodisk array on the metallic substrate.

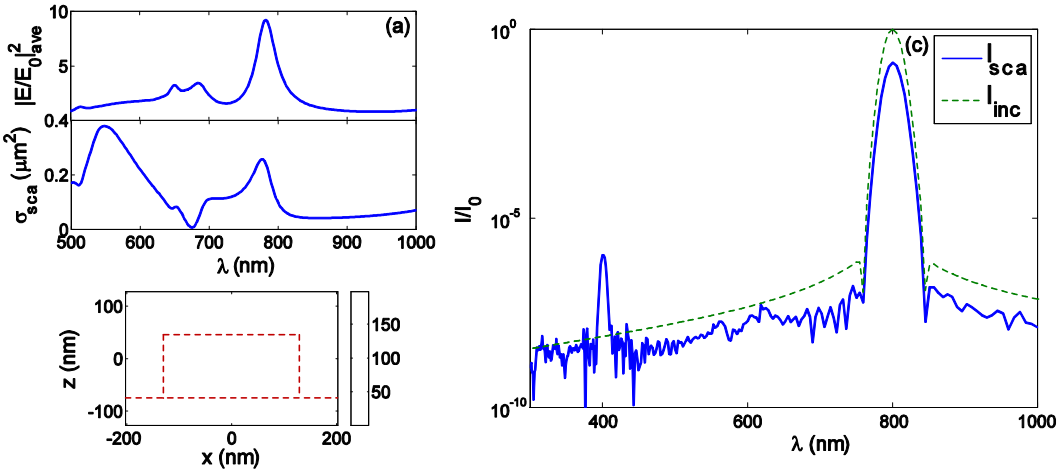

Figure S4. Linear and second-order nonlinear responses of an isolated LN nanodisk on gold substrate. Size and material parameters are the same as in the case of metasurface shown in Figure 2. In (a), the average intensity enhancement $|E/E_0|^2_{ave}$ and the scattering cross-section σ_{sca} are presented. Figure S3b presents the intensity distribution as density colormap in xz-plane and also the electric field distribution as arrows, the lengths of which are proportional to the electric field intensity. In (c), the incidence I_{inc}, reflection I_R, and transmission I_T spectra are shown for pumping condition the same as in Figure 5.

Due to the low intensity enhancement, SHG efficiency η is much low. In isolated LN nanodisk, $\eta = 1.58 \times 10^{-4}$ % (see Figure S4c) for the same pumping condition as in Figure 5, which is two orders-of-magnitude lower than the case of LN metasurface.

S4. Optical responses of metasurfaces of LN nanodisks on reflective dielectric substrates

One might have a question whether the high filed enhancement in LN metasurfaces comes from the reflectivity of metallic substrate. In order to clarify this issue, here we study the optical responses of metasurfaces comprising the LN nanodisks supported by reflective substrates of dielectrics: high-index (Figure S5a) and near-zero-index substrates (Figure S5b). In Figure S5a and S4b, the refractive indices of substrates are 10 and 0.3, respectively. In these cases, weak resonances appear at 716 nm (Figure S5a) and 660 nm (Figure S5b), originating from dipolar Mie resonances (see Figure S4c and S5d).

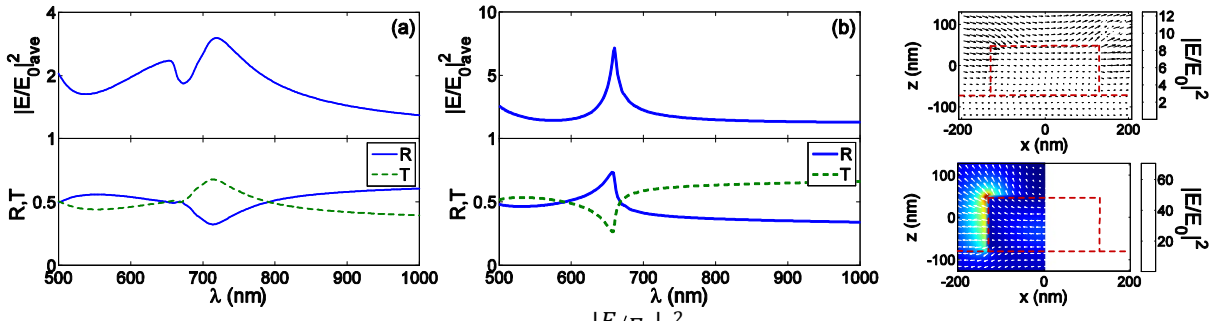

Figure S5. Average intensity enhancement $|E/E_0|^2_{ave}$, reflectance R, and transmittance T in metasurfaces of periodic LN nanodisks supported by the substrates with refractive indices of 10 (a) and 0.3 (b). In (c) and (d), the distributions of intensity (density colormaps) and electric field (arrows) for the case of substrates with indices of 10 (c) and 0.3 (d) are shown, respectively.

Figure S6 presents the results of multipole analyses for the two cases. For the case of substrate with refractive index 10, a broad dipolar band exists at around 716 nm, at which the intensity enhancement has a peak value, with much weaker contributions of magnetic dipole and electric quadrupole (Figure S6a). In contrast, for near-zero-index (0.3) substrate a narrow dipole resonance with a peak at 660 nm contributes to the total optical response of the metasurface (Figure S6b).

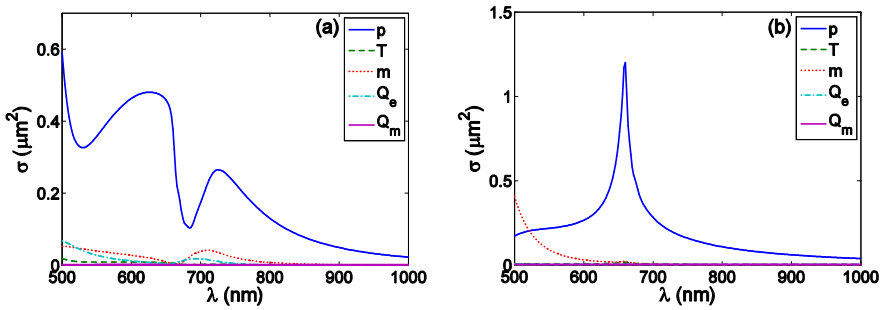

Figure S6. Multipole analyses for metasurfaces of LN nanodisk arrays supported by substrates with refractive indices of 10 (a) and 0.3 (b), respectively. In the insets, p, T, m, Q_e, and Q_m represent the contributions of electric dipole, toroidal dipole, magnetic dipole, electric quadrupole, and magnetic quadrupole, respectively.

S5. Second-harmonic generation from metasurfaces of LN nanorods supported by gold substrate

Metasurfaces of dielectric nanoparticles with various shapes can be used for highly efficient SHG. Here we examine metasurfaces of LN nanorods (Figure S7) instead of nanodisks.

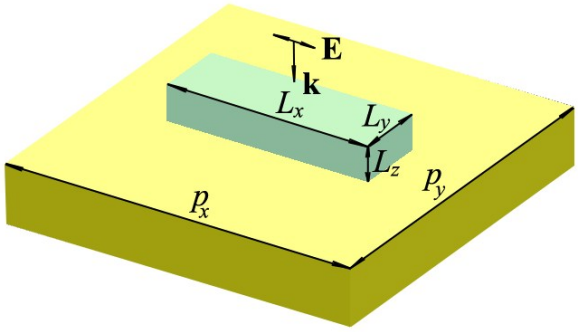

Figure S7. Unit cell of metasurface consisting LN nanorods supported by gold substrate, where p_x and p_y are the periods in x and y directions; L_x, L_y, and L_z are the lengths of LN nanorod along x, y, and z-axes, respectively. The incident light is polarized along x-direction and propagates perpendicular to the metasurface plane.

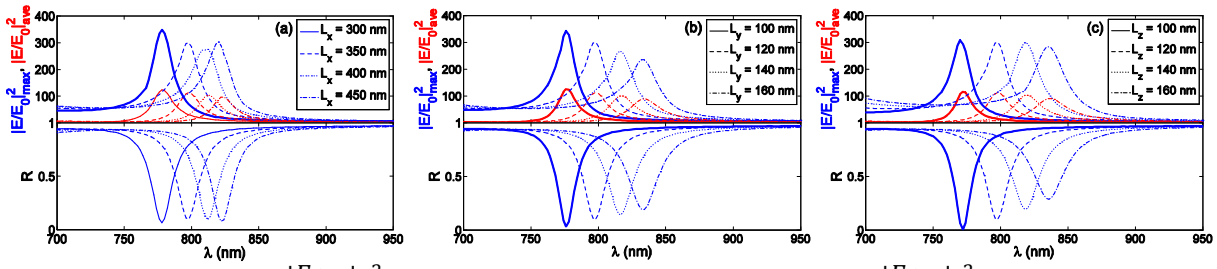

Figure S8. Maximum $|E/E_0|^2_{max}$ and average intensity enhancement $|E/E_0|^2_{ave}$, and reflectance R depending on L_x (a), L_y (b), and L_z (c) in metasurfaces consisting LN nanorods supported by gold substrate. The periods along x- and y-directions are $p_x = 660$ nm and $p_y = 660$ nm, resepectively. Material parameters are the same as in Figure 2. In (a) $L_y = 120$ nm and $L_z = 120$ nm, in (b) $L_x = 350$ nm and $L_z = 120$ nm, in (c) $L_x = 350$ nm and $L_y = 120$ nm, respectively.

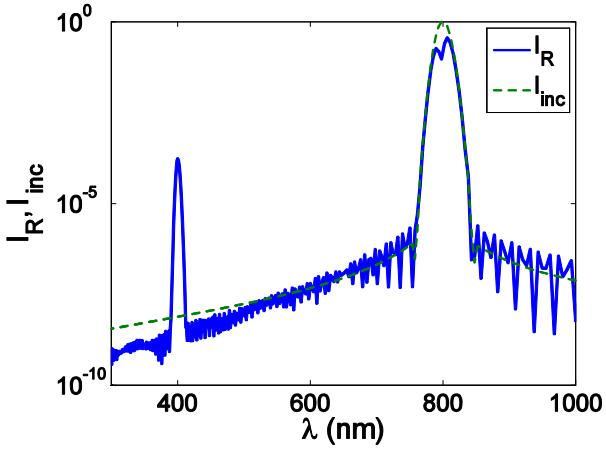

Figure S9. Incidence I_{inc} and reflection spectra I_R from the metasurface of LN nanorods placed on gold substrate. Size parameters for the nanorods are $L_x = 350$ nm, $L_y = 120$ nm, and $L_z = 120$ nm, respectively. Material parameters are the same as in Figure S7. Pumping condition is the same as in Figure 5: the peak intensity is 1.33 GW/cm^2, the duration of pump is 50 fs, and the central wavelength is 800 nm, respectively.

Figure S8 presents the influences of size parameters L_x (a), L_y (b), and L_z (c) on the optical responses of the metasurface of LN nanodisks supported by gold substrate: for the increase nanoparticle size, resonance peak redshifts and broadens as in the case of LN nanodisks. For $L_x = 350$ nm, $L_y = 120$ nm, and $L_z = 120$ nm, the maximum and average intensity enhancement factors at the spectral peak position 798 nm are $|E/E_0|^2_{max} \approx 300$ and $|E/E_0|^2_{ave} \approx 113$, respectively, when the reflectance has the value of $R \approx 0.098$. In the metasurface of the above size parameters, the efficiency of SHG at 400

nm amounts to about $\eta = 1.83 \times 10^{-2}$ % (Figure S9) for pumping condition the same as in Figure 5, which is approximately 1.5 times higher than the case of LN nanodisks, which is attributed to higher field enhancement (see Figure S8).

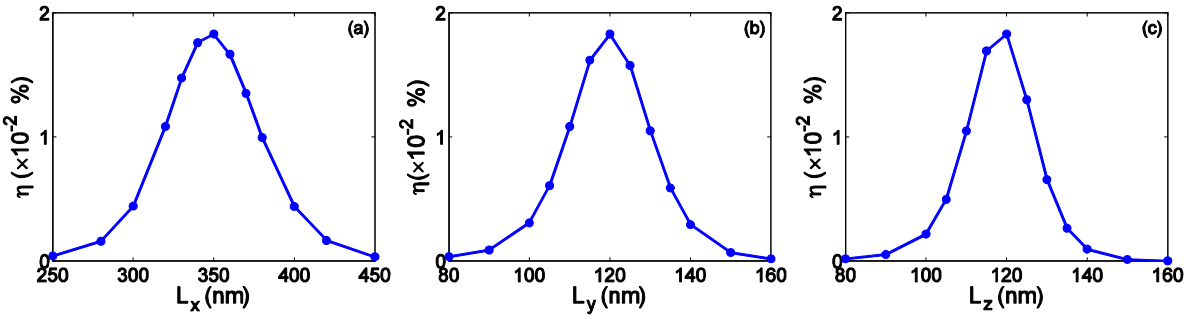

Figure S10. Dependencies of SHG efficiency η on the size parameters L_x (a), L_y (b), and L_z (c). Other structural and material parameters are the same as in Figure S8.

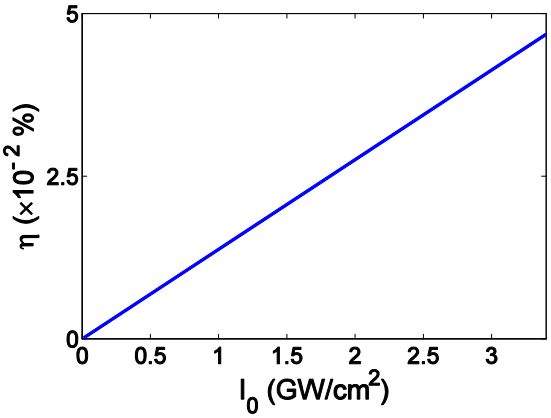

Figure S11. Influence of peak pump intensity I_0 on SHG efficiency η. All the structural and material parameters are the same as in Figure S8.

From Figure S10, we can see that full widths of size parameters at half maxima of SHG efficiency are about $\Delta L_x = 68$ nm, $\Delta L_y = 23$ nm, and $\Delta L_x = 19$ nm, respectively. We can, therefore, obtain high SHG efficiency with size deviations smaller than these values, which are practically feasible with current nanotechnology.

Figure S11 shows the linear dependence of SHG efficiency on the peak intensity I_0 of pump in the metasurface of LN nanorods on gold substrate for $L_x = 350$ nm, $L_y = 120$ nm, and $L_z = 120$ nm,

respectively. At $I_0 = 3.4$ GW/cm^2, SHG efficiency reaches $\eta = 4.68 \times 10^{-2}$ %, similar to the case of metasurface consisting LN nanodisks.

References

[S1] V. A. Zenin, A. B. Evlyukhin, S. M. Novikov, Y. Yang, R. Malureanu, A. V. Lavrinenko, B. N. Chichkov, S. I. Bozhevolnyi, Direct Amplitude-Phase Near-Field Observation of Higher-Order Anapole States. *Nano Lett.* **17**, 7152-7159 (2017).

[S2] K.-H. Kim, W.-S. Rim, Anapole Resonances Facilitated by High-Index Contrast between Substrate and Dielectric Nanodisk Enhance Vacuum Ultraviolet Generation, *ACS Photonics* **5**, 4769-4775 (2018).